A BLIND DEBLURRING AND IMAGE DECOMPOSITION APPROACH FOR ASTRONOMICAL IMAGE RESTORATION

Rahul Mourya [*], *Loïc Denis, Jean-Marie Becker*

Université Jean Monnet,
CNRS, UMR 5516, Laboratoire Hubert Curien,
F-42000, Saint-Étienne, France

Eric Thiébaut

Université de Lyon 1,
CNRS, UMR 5574, Observatoire de Lyon,
F-69561, Saint Genis Laval Cedex, France

ABSTRACT

With the progress of adaptive optics systems, ground-based telescopes acquire images with improved resolutions. However, compensation for atmospheric turbulence is still partial, which leaves good scope for digital restoration techniques to recover fine details in the images. A blind image deblurring algorithm for a single long-exposure image is proposed, which is an instance of *maximum-a-posteriori* estimation posed as constrained non-convex optimization problem. A view of sky contains mainly two types of sources: point-like and smooth extended sources. The algorithm takes into account this fact explicitly by imposing different priors on these components, and recovers two separate maps for them. Moreover, an appropriate prior on the blur kernel is also considered. The resulting optimization problem is solved by alternating minimization. The initial experimental results on synthetically corrupted images are promising, the algorithm is able to restore the fine details in the image, and recover the point spread function.

Index Terms— Astronomical imaging, blind image deblurring, non-convex optimization, alternate minimization, Huber function, ADMM.

1. INTRODUCTION

Acquiring photometrically precise and high resolution images from a ground-based imaging system is highly desirable and remains a long-standing problem in astronomy. The atmospheric turbulence is the major culprit for the distortions in the acquired images. Adaptive optics (AO) [1] partially compensates the turbulence in real-time and brings the effective point-spread-function (PSF) closer to the diffraction limit. However, some amount of blur remains in long-exposure images, and the finest details in the images, which are very important for the astrophysical interpretations, are lost. It is therefore necessary to use image restoration techniques to enhance the quality of the images [2–4].

[*]The author is supported by a PhD grant funded by the ARC6, Région Rhône-Alpes.

Within the isoplanatic domain, the PSF is stationary, and the observed image $\boldsymbol{y}$ formed at the focal plane of the imaging system due to the sought sharp image $\boldsymbol{x}$ can be modeled by the following discretized image formation model:

$$\boldsymbol{y} = \mathcal{P}(\boldsymbol{H}\,\boldsymbol{x}) + \boldsymbol{n} \tag{1}$$

where $\boldsymbol{n}$ is a vector drawn from a white Gaussian distribution, $\mathcal{P}$ denotes a Poisson random process, $\boldsymbol{H}$ is the matrix of discrete convolution from PSF $\boldsymbol{h}$. The image formation model (1) is valid once the scale of image values is expressed in photons, and the background and the flat field corrections have been done on raw observed image.

Recovering $\boldsymbol{x}$ from $\boldsymbol{y}$ even when $\boldsymbol{h}$ is known perfectly is already a difficult inverse problem because the matrix $\boldsymbol{H}$ is often ill-conditioned. It is more realistic to consider that the PSF $\boldsymbol{h}$ is not known perfectly, given the imperfect corrections by AO [5, 6]. Blind image deblurring (BID) is the problem of inferring $\boldsymbol{x}$ from an input $\boldsymbol{y}$ when the $\boldsymbol{h}$ is unknown [7].

Image restoration, in general, has a long history that began in 1950s with astronomical image restoration [3], whereas the development of BID can be traced back to 1970s [8]. BID has been vastly explored for restoring natural images degraded due to motion blur and camera defocus (see [9] and the references within), but only a few are dedicated to astronomical images [4, 8, 10–13]. The BID approaches are specific to the applications, however, most of the successful approaches are built on a Bayesian framework differing primarily in the prior information they include about the image and the blur kernel to restore them.

Contribution: Many astronomical images can be described as a superimposition of two types of components: point-like sources (PS) and extended smooth sources (ES), on a dark background. Image decomposition approaches [14] have been shown to be very useful in image restoration applications. In this paper, we extend the decomposition approach of [15] to the blind deconvolution setting. Different *a priori* are imposed on each component to estimated two separate maps for them. An appropriate *a priori* on the PSF is also imposed. Recovering precisely the position and intensity of PS embedded into ES is of great interest for astronomers. PS are very effective features in the image to precisely estimate

978-0-9928626-3-3/15/$31.00 ©2015 IEEE

the PSF, and thus, when the algorithm progresses to recover precisely the PS, the PSF estimation gets refined, which then ultimately refines the structural details in ES.

2. BLIND IMAGE DEBLURRING

2.1. BID as MAP estimation

Since BID is fundamentally an ill-conditioned and ill-posed problem, strong priors on both the unknown sharp image and the PSF are required to regularize the problem. This naturally leads to *maximum-a-posteriori* (MAP) estimation framework:

$$\{\hat{\boldsymbol{x}}, \hat{\boldsymbol{h}}\}_{\text{MAP}} := \arg\max_{\boldsymbol{x},\boldsymbol{h}} \{p(\boldsymbol{y}|\boldsymbol{x},\boldsymbol{h})\; p(\boldsymbol{x})\; p(\boldsymbol{h})\} \quad (2)$$

which jointly estimates the unknown image and the blur. The likelihood $p(\boldsymbol{y}|\boldsymbol{x},\boldsymbol{h})$ of observed data depends upon the noise statistics, and the prior distributions $p(\boldsymbol{x})$ and $p(\boldsymbol{h})$ impose the prior knowledge about the sought unknowns. Recently, [16] pointed out that MAP approach may completely fail for BID in the absence of a prior on the PSF $\boldsymbol{h}$ favoring some amount of spreading. The authors advocate to use a marginalization approach within a variational Bayesian approximation to estimate more reliably the PSF $\boldsymbol{h}$. In the case of astronomical images, the presence of PS provides both the good starting guess of the PSF and the explicit detection of all point sources of the image during the blind deconvolution procedure helps the MAP approach to succeed, as shown below.

The MAP estimation can equivalently be cast as a minimization problem:

$$\{\hat{\boldsymbol{x}}, \hat{\boldsymbol{h}}\}_{\text{MAP}} := \arg\min_{\boldsymbol{x},\boldsymbol{h}} -\log\{p(\boldsymbol{y}|\boldsymbol{x},\boldsymbol{h})\; p(\boldsymbol{x})\; p(\boldsymbol{h})\} \quad (3)$$

by taking negative $\log$ of equation (2). In the following sections, we specify in detail the each term of equation (3).

2.2. The data fitting term

We consider the non-stationary white Gaussian noise model proposed in [4], which is a pretty accurate approximation for the mix of Poisson and Gaussian noise while keeping the complexity arising in the optimization problem at a moderate level. We believe that sufficiently precise and simple noise model with strict a priori constraints on the solution can result into better behavior of the BID algorithm than a more complex noise model which can hinder in strict enforcement of the constraints. Dropping out the constant terms, the likelihood for the noise model is written as:

$$-\log p(\boldsymbol{y}|\boldsymbol{x},\boldsymbol{h}) = \sum_i \frac{1}{2\sigma_i}\,(\boldsymbol{y}-\boldsymbol{h}*\boldsymbol{x})_i^2 = \frac{1}{2}\|\boldsymbol{y}-\boldsymbol{H}\boldsymbol{x}\|^2_{\boldsymbol{W}}$$

where $\sigma_i = \sigma_i^{ph} + \sigma_i^{det}$, and σ_i^{ph} and σ_i^{det} are *photon* (Poisson) and *detector* (Gaussian) noise variances at the i-th pixel in the image. $\boldsymbol{W}$ is diagonal and is the inverse of the covariance matrix, i.e. $\boldsymbol{W}_{i,i} = 1/\sigma_i$. The covariance matrix depends on $\boldsymbol{x}$ and $\boldsymbol{h}$, thus one could improve its estimate at each iteration of the Algorithm 1 as proposed in [17], but in paper we keep it fixed, and estimate it initially from the observed image as suggested in [4]. For unknown measurements, such as dead or saturated or boundary pixels, $\boldsymbol{W}_{i,i} = 0$, as done for example in [18] for handling boundaries correctly.

2.3. The image regularizer

An astronomical image can be described as the superimposition of point (i.e., unresolved) sources (PS) and extended (i.e., resolved) sources (ES). From a statistical point of view, the PS can be modeled as sparse uncorrelated pixels, and the ES as smoothly varying correlated pixels. Thus, a sparsity inducing ℓ_1-norm is imposed on the PS, and smoothness-inducing edge-preserving Huber prior is imposed on the ES, and two separate maps: $\boldsymbol{x}_P$ and $\boldsymbol{x}_E$, are estimated . An important physical constraint, the positivity of these maps, is also imposed, and the *a priori* on PS and ES are written as:

$$-\log p(\boldsymbol{x}_P) = \lambda\|\boldsymbol{x}_P\|_1, \quad \boldsymbol{x}_P \geq 0$$

$$-\log p(\boldsymbol{x}_E) = \mu\sum_i \phi_\delta(\nabla_i\,\boldsymbol{x}_E), \quad \boldsymbol{x}_E \geq 0$$

where $\phi_\delta(t) = \begin{cases} \frac{1}{2}\|t\|_2^2 & \|t\|_2 \leqslant \delta \\ \delta(\|t\|_2 - \frac{\delta}{2}) & \|t\|_2 > \delta, \end{cases}$

and $\nabla_i\,\mathbf{x} \in \mathbb{R}^2$ represents the gradient vector at the i-th pixel of the image. $\{\lambda,\mu\} > 0$ are tunable hyperparameters, and $\delta \geq 0$ is a threshold. The prior on ES is an intermediate between Total Variation and Sobolev regularization, and its behavior is adjusted by the δ.

2.4. The PSF regularizer

For ground-based large telescopes, there are mainly two regimes of imaging: long and short (less than $\approx 1/4$ second) exposures. Short exposure images take the form of speckle patterns, consisting of multiple distorted and overlayed copies of the diffraction-limited PSF. In order to increase the signal-to-noise ratio, almost all astronomical imaging is performed with long exposures, unless conditions (such as high sky brightness in the infrared) prevent it. Because the short-exposure PSFs are highly variable, both in structure and centroid position, the summed long-exposure PSF is highly blurred compared to the diffraction-limit, even with a good seeing conditions. Thanks to the real-time correction of the AO system, the long-exposure PSF is maintained closer to diffraction-limit, but because of some remaining perturbations in the imaging system, the effective PSF still has some uncorrected parts. Several measurements of PSF done at Gemini north and Keck observatory [6] reveal that the uncorrected part of the PSF are approximately Lorentzian or Gaussian shape or both atop the Airy pattern. The PSF of the AO corrected imaging system is quite smooth with small aberrations, thus a smoothness inducing Sobolev-norm on the sought PSF is chosen as *a priori* on PSF. The PSF of the considered imaging system is always positive, upper bounded by the peak value of the diffraction-limited PSF, and normalized, thus the *a priori* on PSF is written as:

$$-\log p(\boldsymbol{h}) = \frac{\nu}{2}\|\nabla\boldsymbol{h}\|_2^2,\; 0 \leq \boldsymbol{h} \leq \alpha,\; \mathbf{1}^T\boldsymbol{h} = 1.$$

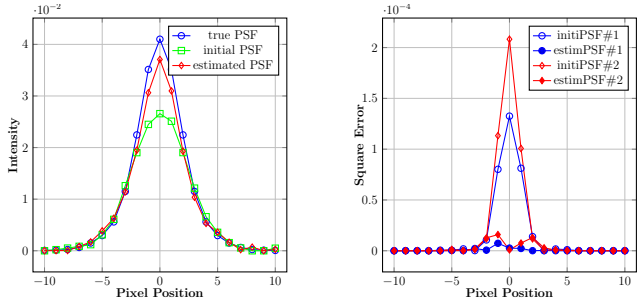

Fig. 1: Left to right: Profile of the PSFs used for BID illustration on the image at the bottom row in Figure 3, Square error profiles of the initial PSFs and the estimated PSFs with respect to the true PSFs. PSF#1 and PSF#2 correspond to the PSFs used for the top row and the bottom row in Figure 3 respectively.

where α is the peak value of Airy pattern for a given aperture, and $\gamma > 0$ is hyperparameter.

2.5. BID as a constrained optimization problem

With all prior terms described in preceding sections, BID is expressed as a constrained minimization problem:

$$\{\hat{\boldsymbol{x}}_P, \hat{\boldsymbol{x}}_E, \hat{\boldsymbol{h}}\}_{\text{MAP}} := \arg \min_{\boldsymbol{x}_P, \boldsymbol{x}_E, \boldsymbol{h}} \frac{1}{2}\|\boldsymbol{y} - \boldsymbol{H}\boldsymbol{x}\|^2_{\boldsymbol{W}} + \lambda\|\boldsymbol{x}_P\|_1 + \mu \sum_i \phi(\nabla \boldsymbol{x}_E)_i + \frac{\nu}{2}\|\nabla \boldsymbol{h}\|_2^2$$
$$\texttt{s.t.}\ \boldsymbol{x}_P + \boldsymbol{x}_E = \boldsymbol{x},\ \boldsymbol{x}_P \geq 0,\ \boldsymbol{x}_E \geq 0,$$
$$0 \leq \boldsymbol{h} \leq \alpha,\ \boldsymbol{1}^T\boldsymbol{h} = 1. \qquad (4)$$

This is a difficult large-scale non-convex optimization problem with non-differentiable terms, and still may have several local minima even though we restrict its solution space with the possible penalties and constraints. Few authors [12] propose to solve BID by a joint estimation approach (estimating simultaneously both $\boldsymbol{x}$ and $\boldsymbol{h}$), but their formulations of BID are comparatively simpler, and do not contain any non-differentiable terms. Solving this problem by joint estimation approach is a very difficult task, however, the problem is convex with respect to each of the unknown when considering the other fixed, thus, a much simpler and widespread approach is to perform *Alternating Minimization* [19], as presented in Algorithm 1. One can reach to the expected local minimum using Algorithm 1, provided that one starts with a good initial guess of the PSF. Luckily, in case of astronomical imaging, finding a good initial guess of the PSF is not a tedious task, one can extract it from the observed image itself by selecting few blurry point-like sources (reference stars), otherwise one could ask for calibrated PSF from the astronomers: they always have model fitted PSF to characterize their imaging system. The calibrated PSF of an imaging system with AO are quite close to the true PSF. The optimization problems (5) and (6) in Algorithm 1 are solved by the variable splitting

Algorithm 1: Blind Deblurring Algorithm

Data: $\boldsymbol{y}$, $\boldsymbol{W}$, and $\{\lambda, \mu, \delta, \gamma\}$.
Result: $\{\hat{\boldsymbol{x}}, \hat{\boldsymbol{h}}\}$
Initialization: $\mathbf{h} = \mathbf{h}^{(0)}$; $t = 1$;
while *convergence not reached* **do**

Image Estimation:

$$\{\hat{\boldsymbol{x}}_P^{(t+1)}, \hat{\boldsymbol{x}}_E^{(t+1)}\} := \arg \min_{\boldsymbol{x}_P, \boldsymbol{x}_E} \{\frac{1}{2}\|\boldsymbol{y} - \boldsymbol{H}\boldsymbol{x}\|^2_{\boldsymbol{W}} + \lambda\|\boldsymbol{x}_P\|_1 + \mu \sum_i \phi(\nabla_i \boldsymbol{x}_E)\}$$
$$\texttt{s.t.}\quad \boldsymbol{x}_P + \boldsymbol{x}_E = \boldsymbol{x},\quad \boldsymbol{x}_P \geq 0,\quad \boldsymbol{x}_E \geq 0. \qquad (5)$$

PSF Estimation:

$$\hat{\boldsymbol{h}}^{(t+1)} := \arg\min_{\mathbf{h}} \{\frac{1}{2}\|\boldsymbol{y} - \boldsymbol{X}\boldsymbol{h}\|^2_{\boldsymbol{W}} + \frac{\nu}{2}\|\nabla \boldsymbol{h}\|_2^2\}$$
$$\texttt{s.t.}\quad \boldsymbol{1}^T\boldsymbol{h} = 1,\quad 0 \leq \boldsymbol{h} \leq \alpha. \qquad (6)$$

$t = t + 1$
return: $\hat{\boldsymbol{x}}$, $\hat{\boldsymbol{h}}$,

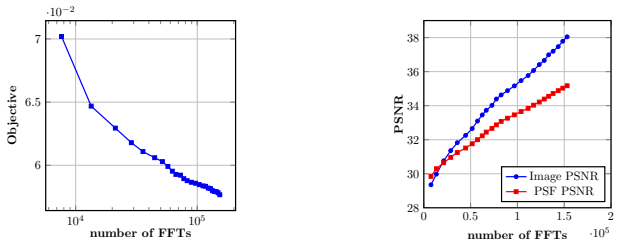

Fig. 2: Convergence of the proposed BID for the image shown at bottom row in Figure 3: Left to right: Cost, and Image and PSF PSNR vs number of FFTs

trick, and transforming the resulting constrained optimization problem into an unconstrained problem by forming the augmented Lagrangian. The solution is then found by minimizing the augmented Lagrangian by the convex optimization framework recently proposed in [20]. We introduce the variables splittings: $\boldsymbol{x}_P - \boldsymbol{z}_P = 0$ and $\nabla \boldsymbol{x}_E - \boldsymbol{z}_E = 0$, and transform the problem (5) into following unconstrained form:

$$\min_{\boldsymbol{x}_P, \boldsymbol{x}_E, \boldsymbol{z}_P, \boldsymbol{z}_E, \boldsymbol{u}_P, \boldsymbol{u}_E} \{\frac{1}{2}\|\boldsymbol{y} - \boldsymbol{H}\boldsymbol{x}\|^2_{\boldsymbol{W}} + g(\boldsymbol{x}_P) + \lambda\|\boldsymbol{z}_P\|_1 + \frac{\rho_1}{2}\|\boldsymbol{x}_P - \boldsymbol{z}_P + \boldsymbol{u}_P\|_2^2 + \mu \sum_i \phi(\nabla_i \boldsymbol{z}_E) + g(\boldsymbol{x}_E) + \frac{\rho_2}{2}\|\nabla \boldsymbol{x}_E - \boldsymbol{z}_E + \boldsymbol{u}_E\|_2^2\}$$

where g is an indicator function for positivity, $\{\boldsymbol{u}_P, \boldsymbol{u}_E\}$ are scaled Lagrangian multipliers, and $\{\rho_1, \rho_2\} > 0$ are called *penalty parameters*.

Similarly, we introduce the variable splitting: $\boldsymbol{h} - \boldsymbol{z} = 0$, and transform the problem (6) into the unconstrained form:

$$\min_{\boldsymbol{h}, \boldsymbol{z}, \boldsymbol{u}} \{\frac{1}{2}\|\boldsymbol{y} - \boldsymbol{X}\boldsymbol{h}\|^2_{\boldsymbol{W}} + f_1(\boldsymbol{h}) + f_2(\boldsymbol{z}) + \frac{\rho_3}{2}\|\boldsymbol{h} - \boldsymbol{z} + \boldsymbol{u}\|_2^2\}$$

where $\boldsymbol{X}$ is the discrete convolution matrix formed from the

image $\boldsymbol{x}$, and f_1, f_2 are the indicator functions for the bound and the probability simplex constraints, respectively. Again, $\rho_3 > 0$ is the *penalty parameter*, and $\boldsymbol{u}$ is scaled Lagrangian multiplier. The *penalty parameters* are selected by hand to achieve fast convergence speed, however a very large range of values offer satisfactory convergence speed, as shown in [20]. The iterations for each of the problems are terminated once the relative change in the cost function is sufficiently low, and similarly, the outer iteration in Algorithm 1 is terminated once the relative change in cost function (4) is sufficiently low.

2.6. The hyperparameters

The proposed BID includes three tunable hyperparameters: $\{\lambda, \mu, \nu\} \geq 0$, and a tunable threshold: $\delta \geq 0$. The hyperparameters balance between the likelihood term and the priors, and their values are proportional to noise variance in the observed image. Hyperparameter λ controls the sparsity in the PS map, μ and δ control the smoothness and sharp edges in the ES map, and the ν controls the smoothness of the PSF. A good balance among the hyperparameters is essential to obtain satisfactory decomposition into PS and ES maps, and the final result, however finding optimal values for them is a non-trivial task, but at same time it makes the BID flexible. If one believes that the observed image contains only PS, then one can mask out the ES setting $\mu \to \infty$ (and conversly $\lambda \to \infty$ to suppress point sources), or by trivially modifying the algorithm. In our experimental results, we chose the hyperparameters heuristically after few trials.

3. EXPERIMENTAL RESULTS

We evaluate the proposed BID algorithm on numerical simulations of a simplified astronomical scene and of an observed scene obtained from a space telescope. The top row in Figure 3 shows BID results on the synthetic scene consisting of numerous point-like sources made of single pixels, and extended sources made of few small Lorentzian discs and large bivariate-Gaussians in different orientations, all on a dark background. The bottom row in Figure 3 shows BID results on the simulation involving a real image captured by Spitzer space telescope. We consider an image captured by a space telescope because it is distorted only due to imperfections in the imaging system, but not by the atmospheric turbulence. Both the synthetic and the astronomical images have high dynamic ranges, but have been scaled to the $[0, 1]$ range. The PSF considered here is a typical example of Gemini north 8.1 m telescope, which has been generated here by the convolution between an Airy pattern of radius 1.5 pixels and a Gaussian with FWHM = $[3.5, 4]$ pixels [6]. The simulated blurred images are created by synthetically blurring the two images with this PSF, and then corrupting them with a mixture of Poisson and white Gaussian noise. The blurred images are scaled to the range 0 to 10^5 photons before adding Poisson noise, and rescaled back to the range 0 and 1 before adding white Gaussian noise of variance 10^{-3}.

To apply the proposed BID method on the simulated data, few (4 to 5) blurry point-like looking sources in the observed image are extracted, aligned, stacked, and averaged to get the initial guess of the PSF. The inner iterations and outer iterations in Algorithm 1 are terminated when the relative change in function cost reaches 10^{-6}. The three hyperparameters in the proposed BID are tunned by hand after few trials to reach a satisfying image quality.

Improvement in PSNR for the estimated image and estimated PSF for the image in top row of Figure 3 is 8.5dB and 4.5dB, and for the image in bottom row is 8.47dB and 12.44dB respectively.

To check the viability/advantage of the map decomposition in the proposed BID, we applied BID on the image shown in top row in Figure 3 with only the *a priori* for the ES (keeping λ very large, and tuning μ and δ to achieve the best deblurring quality), as expected the improvement in PSNR for the estimated image and PSF reach only up to 5.45dB and 6.58dB respectively, which is significantly below the values obtained when the decomposition is applied. To have a single component, if we tune the hyperparameters to achieve good resolution of the point sources then the smooth extended source are deteriorated, and vice-versa is also observed.

4. CONCLUSION

This paper described a blind deconvolution method well fitted to astronomical image restoration. The presence of unresolved point sources are very helpful to estimate the blur in an astronomical image. The proposed method, thus, jointly performs the detection of point-like objects and the reconstruction of extended objects. This is achieved by decomposing the sought image into two components using different regularization terms on each component. By alternating between estimation of the PSF and deblurring, and decomposition into the two components, the method progressively reaches a satisfactory result. We showed on some numerical simulations that the method can successfully perform the decomposition into point-source and extended object, and recover correctly the PSF. Performing the decomposition clearly helps in correctly modeling astronomical scenes, as observed when comparing the restoration quality obtained with and without the decomposition. Ongoing works are carried on the application of the method to ground-based blurry images.

REFERENCES

[1] R. Davies and M. Kasper, "Adaptive Optics for Astronomy," *Annu. Rev. Astron. Astrophys.*, vol. 50, pp. 305–351, 2012.

[2] G. R. Ayers and J. C. Dainty, "Iterative blind deconvolution and its applications," *Opt. Lett.*, vol. 13, pp. 547–549, 1988.

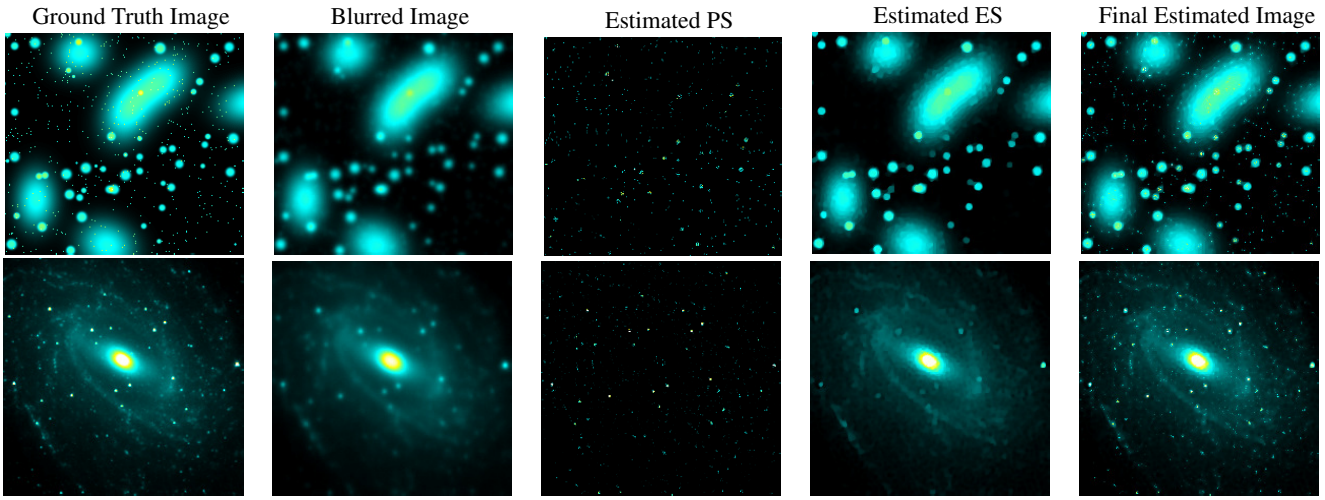

Fig. 3: Illustration of the proposed BID. On the top row for synthetic scene, and the bottom row for the galaxy NGC6744 (the image obtained from Spitzer Heritage Archive). Parameters used for the restoration: for top row: λ =1E-4, μ =5E-2, δ =2.5E-3, ν =5E-1, and 35 outer iterations; for bottow row: λ =4E-5, μ =7E-3, δ =5E-3, ν =2.5E0, and 25 outer iterations.

[3] R. Molina, J. Núñez, and F. J. Cortijo, "Image Restoration in Astronomy:A Bayesian Perspective," *IEEE Signal Processing Magazine*, vol. 18, no. 2, pp. 11–29, 2001.

[4] L. M. Mugnier, T. Fusco, and J-M. Conan, "MISTRAL: a myopic edge-perserving image restoration method, with application to astronomical adaptive-optics-corrected long-exposure images," *J. Opt. Soc. Am. A*, vol. 21, pp. 1841–1854, 2004.

[5] F. J. Rigaut, B. L. Ellerbroek, and R. Flicker, "Principles, limitations, and performance of multiconjugate adaptive optics," in *Astronomical Telescopes and Instrumentation*. International Society for Optics and Photonics, 2000, pp. 1022–1031.

[6] J. Drummond et al., "The Adaptive Optics Point Spread Function from Keck and Gemini," in *AMOS Technical Conference*, Maui,Hawaii, 2009, pp. 1–9.

[7] D. Kundur and D. Hatzinakos, "Blind Image Deconvolution: A Algorithmic Approach to Practical Image Restoration," *IEEE Trans. Sig. Proc.*, vol. 13, no. 3, pp. 43–64, 1996.

[8] M. Cannon, "Blind deconvolution of spatially invariant image blurs with phase," *IEEE Trans. on Acoustics, Speech and Signal Processing*, vol. 24, no. 1, pp. 58 – 63, 1976.

[9] M. S. C. Almeida and L. B. Almeida, "Blind and Semi-Blind Deblurring of Natural Images," *IEEE Trans. on Image Processing*, vol. 19, no. 1, pp. 36–52, 2010.

[10] T Schulz, B Stribling, and J Miller, "Multiframe blind deconvolution with real data: imagery of the Hubble Space Telescope.," *Optics express*, vol. 1, no. 11, pp. 355–62, Nov. 1997.

[11] É. Thibaut and J.-M. Conan, "Strict a priori constraints for maximum likelihood blind deconvolution," *JOSAA*, vol. 12, no. 3, pp. 485–492, March 1995.

[12] E. Thiébaut, "Optimization issues in blind deconvolution algorithms," in *Proc. SPIE 4847, Astronomical Data Analysis II*, Waikoloa, Hawai'i, 2002, number 0, SPIE.

[13] S. Harmeling, M. Hirsch, S. Sra, and B. Schölkopf, "Online blind deconvolution for astronomical imaging," in *IEEE Int. Conf. Comput. Photogr.*, San Francisco, CA, 2009, pp. 1–7.

[14] J.-L. Stark, M. Elad, and D. Donoho, "Image decomposition via the combination of sparse representations and a variational approach," *IEEE Trans. on Image Processing*, vol. 14, no. 10, pp. 1570–1582, 2005.

[15] J.-F. Giovannelli and A. Coulais, "Positive deconvolution for superimposed extended source and point sources," *Astron. Astrophys.*, vol. 439, no. 1, pp. 401 – 412, 2005.

[16] A. Levin, Y. Weiss, F. Durand, and W. T. Freeman, "Understanding blind deconvolution algorithms," *IEEE Trans. on Pattern Analysis Machine Intelligence*, vol. 33, no. 12, pp. 2354–2367, 2011.

[17] Jia Li, Zuowei Shen, Rujie Yin, and Xiaoqun Zhang, "A reweighted l2 method for image restoration with poisson and mixed poisson-gaussian noise," Tech. Rep., UCLA Preprint, 2012. 68, 106, 2012.

[18] A. Matakos, S. Ramani, and J. A. Fessler, "Accelerated edge-preserving image restoration without boundary artifacts," *IEEE Trans. on Image Processing*, vol. 22, no. 5, pp. 2019–2029, 2013.

[19] T. F. Chan and C.K. Wong, "Convergence of the alternating minimization algorithm for blind deconvolution," *Linear Algebra and its Applications*, vol. 316, pp. 259 – 285, 2000.

[20] R. Mourya, L. Denis, J-M. Becker, and E. Thiébaut, "Augmented Lagrangian without alternating directions: Practical algorithms for inverse problems in imaging," *preprint:* `https://hal-ujm.archives-ouvertes.fr/ujm-01122878`, Jan. 2015.